

---

# Dynamics of small bodies in planetary systems

Mark C. Wyatt

Institute of Astronomy, University of Cambridge, Cambridge CB3 0HA, UK  
wyatt@ast.cam.ac.uk

The number of stars that are known to have debris disks is greater than that of stars known to harbour planets. These disks are detected because dust is created in the destruction of planetesimals in the disks much in the same way that dust is produced in the asteroid belt and Kuiper belt in the solar system. For the nearest stars the structure of their debris disks can be directly imaged, showing a wide variety of both axisymmetric and asymmetric structures. A successful interpretation of these images requires a knowledge of the dynamics of small bodies in planetary systems, since this allows the observed dust distribution to be deconvolved to provide information on the distribution of larger objects, such as planetesimals and planets. This chapter reviews the structures seen in debris disks, and describes a disk dynamical theory which can be used to interpret those observations. In this way much of the observed structures, both axisymmetric and asymmetric, can be explained by a model in which the dust is produced in a planetesimal belt which is perturbed by a nearby, as yet unseen, planet. While the planet predictions still require confirmation, it is clear that debris disks have the potential to provide unique information about the structure of extrasolar planetary systems, since they can tell us about planets analogous to Neptune and even the Earth. Significant failings of the model at present are its inability to predict the quantity of small grains in a system, and to explain the origin of the transient dust seen in some systems. Given the complexity of planetary system dynamics and how that is readily reflected in the structure of a debris disk, it seems inevitable that the study of debris disks will play a vital role in our understanding of extrasolar planetary systems.

## 1 Introduction

Planetary systems are not just made up of *planets*, but are also composed of numerous small bodies ranging from asteroids and comets as large as 1000 km down to sub- $\mu\text{m}$ -sized dust grains. In the solar system the asteroids and

comets are confined to relatively narrow rings known as the asteroid belt and the Kuiper belt (see chapters by Nakamura and Jewitt). These belts are the source of the majority of the smaller objects seen in the solar system, since such objects are inevitably created in collisions between objects within the belts (see chapter by Michel). Sublimation of comets as they are heated on approach to the Sun is another source of dust in the solar system.

It is known that extrasolar systems also host belts of planetesimals (a generic name for comets and asteroids) that are similar to our own asteroid belt and Kuiper belt. These were first discovered using far-IR observations of nearby stars, which showed excess emission above that expected to come from the stellar photosphere [5]. This emission comes from dust that is heated by the star and which re-radiates that energy in the thermal infrared, at temperatures between 40-200 K, depending on the distance of the dust from the star. The lifetime of the dust is inferred to be short compared with the age of the star, and so it is concluded that the dust cannot be a remnant of the proto-planetary disk that formed with the star (see chapter by Takeuchi), rather it must originate in planetesimal belts much in the same way that dust is created in the solar system [7].

Over 300 main sequence stars are now known with this type of excess emission [50, 74, 10], and such objects are either known as Vega-like (after the first star discovered to have this excess), or as debris disks. Statistical studies have shown that  $\sim 15\%$  of normal main sequence stars have debris disks, although it should be stressed that the disks which can be detected with current technology have greater quantities of dust than is currently present in the solar system by a factor of at least 10 [25]. Nevertheless this indicates that debris disks are common, more common in fact than extrasolar planets which are found around  $\sim 6\%$  of stars [18]. Studying these disks provides a unique insight into the structure of the planetary systems of other stars. Indeed, the nearest and brightest debris disks can be imaged, and such studies have provided the first images of nearby planetary systems. These images reveal the distribution of dust in the systems, which can in turn be used to infer the distribution of parent planetesimals, and also the architecture of the underlying planetary system. However, to do so requires an understanding of both the mechanism by which dust is produced in planetesimal belts and its consequent dynamical evolution, as well as of the dynamical interaction between planets and planetesimals and between planets and dust.

This chapter reviews our knowledge of debris disks from observations (§2) and describes a simple model for planetesimal belt evolution which explains what we see (§3), as well as how the detailed interaction between planets and planetesimals imposes structure on that planetesimal belt (§4), and how those perturbations translate into structures seen in the dust distribution (§5). Conclusions, including what has been learned about the planetary systems of nearby stars from studying these disks, are given in §6.

## 2 Observed debris disk structures

The debris disks with well resolved structure are summarised in Table 1.<sup>1</sup> There are two types of debris disk structure: axisymmetric structure (i.e., dust or planetesimal surface density as a function of distance from the star), and asymmetric structure (i.e., how that surface density varies as a function of azimuth). I will deal with each of these in turn.

**Table 1.** Summary of observed properties of debris disks the structure of which has been significantly resolved at one wavelength or more. Asymmetries are identified as: W=Warp, C=Clump, S=Spiral, B=Brightness asymmetry, O=Offset, H=Hot dust component, N=No discernible asymmetry.

Name	Sp Type	Age, Myr	$r$ , AU	$i$ , °	$f = L_{\text{ir}}/L_{\star}$	Asymm	Ref
HD141569	B9.5e	5	34 – 1200	35	$84 \times 10^{-4}$	S	[17, 12]
HR4796	A0V	8	60 – 80	17	$50 \times 10^{-4}$	B	[67, 76]
$\beta$ Pictoris	A5V	12	10 – 1835	$\sim 3$	$26 \times 10^{-4}$	WC	[29, 28, 77]
HD15115	F2V	12	31 – 554	$\sim 0$	$5 \times 10^{-4}$	B	[37]
HD181327	K2V	12	68 – 104	58	$25 \times 10^{-4}$	N	[69]
AU Mic	M1Ve	12	12 – 210	$\sim 0$	$6 \times 10^{-4}$	WC	[48]
HD32297	A0V	< 30	40 – 1680	10	$27 \times 10^{-4}$	B	[33]
HD107146	G2V	100	80 – 185	65	$12 \times 10^{-4}$	N	[2]
HD92945	K1V	100	45 – 175	29	$8 \times 10^{-4}$	N	[21]
Fomalhaut	A3V	200	133 – 158	24	$0.8 \times 10^{-4}$	(CB)O	[30, 71, 35]
HD139664	F5V	300	83 – 109	< 5	$0.9 \times 10^{-4}$	N	[36]
Vega	A0V	350	90 – 800	$\sim 90$	$0.2 \times 10^{-4}$	C	[29, 38, 73, 51]
$\epsilon$ Eridani	K2V	850	40 – 105	65	$0.8 \times 10^{-4}$	CO	[26]
$\eta$ Corvi	F2V	1000	1.5, 150	45	$5.3 \times 10^{-4}$	CH	[93]
HD53143	K1V	1000	55 – 110	45	$2.5 \times 10^{-4}$	N	[36]
$\tau$ Ceti	G2V	10000	$\sim 55$	60-90	$0.3 \times 10^{-4}$	N	[25]

### 2.1 Axisymmetric structure

The most basic information about the structure of a debris disk that we can obtain is the distance of the dust from the star. This can be deduced without resolving the dust location by looking at the Spectral Energy Distribution (SED), since this indicates the temperature of the dust, which by thermal balance with the stellar luminosity tells us its distance from the star. For black body dust

<sup>1</sup> Resolved disks have also been reported for the following stars: HD92945, HD61005, HD10647, HD202917, and HD207129 (see <http://astro.berkeley.edu/~kalas/lyot2007/agenda.html>), and HD15745 (Kalas et al., ApJ, submitted). I have excluded these images from the discussion, since they have yet to appear in the literature at the time of writing.

$$T_{\text{bb}} = 278.3L_{\star}^{0.25}/\sqrt{r}, \quad (1)$$

where  $L_{\star}$  is in  $L_{\odot}$  and  $r$  is distance from star in AU. Thus dust location,  $r$ , can be estimated as long as the level of dust emission has been measured at two or more wavelengths from which its temperature can be estimated.

However, such estimates suffer large uncertainties, since the exact temperature of the dust depends on its size and composition (see chapter by Li). Assuming black body emission for the grains can underestimate (or overestimate) the distance of the dust from the star by a factor of 3 or more if the dust is small [69], since small grains emit inefficiently at long wavelengths and so attain equilibrium temperatures that are significantly higher than black body [91]. Likewise, an SED which can be fitted by a black body emission spectrum does not necessarily indicate that all of the dust is at a single distance from the star, any more than one that requires multiple temperatures indicates that the disk is broad, since dust at multiple distances can appear to have one temperature, and dust with a range of sizes at the same distance from the star have a range of temperatures [53]. This underlines the fact that the interpretation of SEDs is degenerate, and that in order to determine the radial structure of a disk it needs to be spatially resolved. On the other hand, once the radial location of the dust is known the information in the SED is extremely valuable, since it allows a determination of the emission properties of the grains, and hence of their size and/or composition [90, 45].

Nevertheless, it seems that the majority of the known debris disks have SEDs that are dominated by dust at a single temperature, and are seen in images to be dominated by dust at a distance from the star that is compatible with that temperature. More often than not that distance is  $> 30$  AU from the star, which means that debris disks are analogous to our own Kuiper belt [92]. Naturally, the fact that these disks have inner holes similar in size to the planetary system in our solar system leads to the intriguing possibility that there is an (as yet) unseen planetary system sweeping these regions free of both planetesimals and dust. I will return to the putative planetary system in §4. Here I simply note that while these inner holes are usually dust free [82], a few systems are known with dust within this hole, such as  $\eta$  Corvi [93] and Vega [1]. The hot dust in these systems is thought to be transiently regenerated [94], and care would need to be taken when interpreting observations of the hot dust within the framework described in this chapter (see §6).

Exactly how broad these disks are is a matter for debate. Optical imaging suggests that there are two types of disk, narrow and broad [36]. However, detectability may be an issue in some cases, since a disk's outer edge is often difficult to detect, as the fraction of intercepted starlight falls off with radius, much in the same way that it was not known for a long time whether or not the outer edge of the Kuiper belt is abrupt [80]. Some disks clearly are extended though, such as that of  $\beta$  Pictoris, which is seen to extend out to  $> 1000$  AU in optical imaging [70], but which is seen as close in as  $10 - 20$  AU in mid-IR imaging [77]. While disks with a dust distribution as broad

as that of  $\beta$  Pictoris are rare, the presence of dust at large distances from the star is becoming more common-place. It is now known that dust in the archetypal debris disk Vega is not confined to  $\sim 90$  AU as suggested by sub-mm images [29]. Rather the dust distribution seen at 24 and 70  $\mu\text{m}$  extends out to 800 AU [73]. This defies intuition, since if the dust is at a range of distances, the disk should appear smaller at the shorter wavelengths (since shorter wavelengths tend to probe hotter dust). This intuitive behaviour is indeed seen in the disk of Fomalhaut [71]. It is thought that the counter-intuitive behaviour of Vega's disk arises because the grain size distribution changes with distance: the dust seen at large distances is small, of order a few  $\mu\text{m}$ , and so is heated above black body and emits very inefficiently in the sub-mm, whereas that seen at  $\sim 90$  AU is large, mm- to cm-sized, and emits efficiently in the sub-mm at (relatively low) black body-like temperatures. A similar change in size distribution with distance is seen in the extended dust distributions of  $\beta$  Pictoris and AU Mic. The extension of these disks is not seen in mid- and far-IR images, but in optical and near-IR images of scattered starlight, and the colours and polarisation of the scattered light show that the dust at large distances in these systems is small, sub- $\mu\text{m}$  in size [23].

## 2.2 Asymmetric structure

While to first order debris disks are rings of material, even if the location and breadth of the rings is wavelength dependent, on closer inspection those that have been imaged with sufficient clarity also exhibit significant asymmetries. Different types of asymmetries have been identified which can be grouped into the following categories: warps, spirals, offsets, brightness asymmetries, and clumps. The observed structures are summarised in Fig. 1 and are discussed in more detail below.

### Warps

A warp arises when the plane of symmetry of a disk varies with distance from the star. It is only edge-on extended debris disks for which a warp can be seen, since this orientation allows the plane of symmetry at any given distance to be readily identified with the location of the maximum surface brightness there. Both of the edge-on disks with significant extension,  $\beta$  Pictoris and AU Mic, are warped [28, 48], as is the structure of the zodiacal cloud in the solar system [91]. Recent observations of  $\beta$  Pictoris suggest that its warp may in fact not be continuous, and that there are two separate disks with different planes of symmetry [20]. Since the images which show warps in debris disks have been made in scattered light, it is important to point out that care must be (and has been) taken when interpreting these observations, since asymmetric scattering (i.e., the effect that causes back scattering to be stronger than forward scattering) can introduce perceived asymmetries into observations of an otherwise axisymmetric disk [34]. A warp has also been identified in the

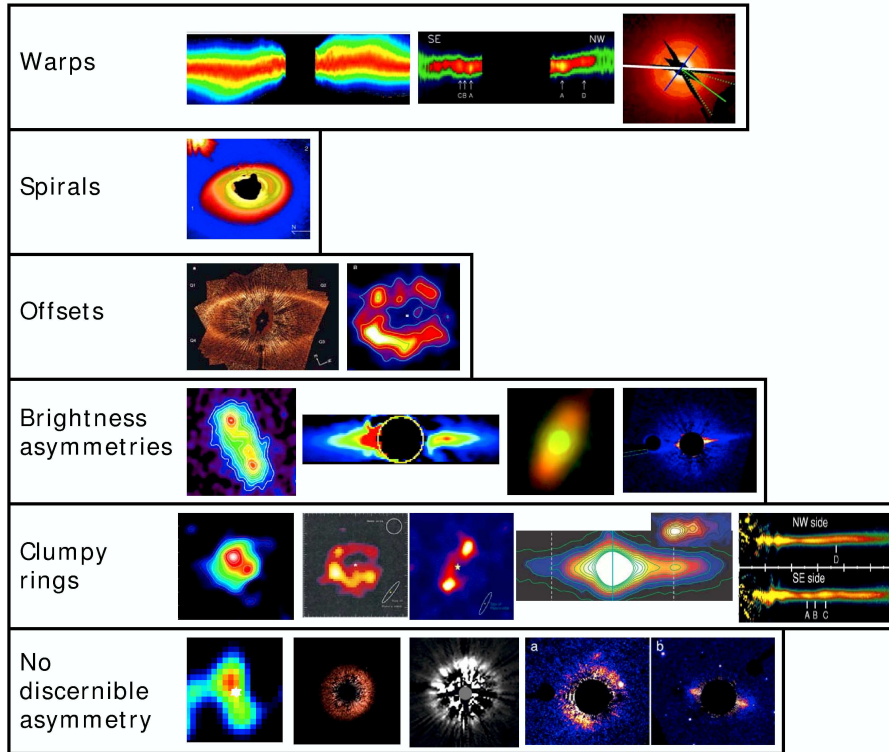


**Fig. 1.** Summary of asymmetries seen in the structures of debris disks. References for the images are from left to right: warps ( $\beta$  Pictoris [28], AU Mic reprinted with permission from AAAS [48], TW Hydra [65]); spirals (HD141569 [12]); offsets (Fomalhaut reprinted by permission from Macmillan Publishers Ltd: Nature [35] copyright 2005,  $\epsilon$  Eridani [26]); brightness asymmetries (HR4796 [76], HD32297 [68], Fomalhaut [71], HD15115 [37]); clumpy rings (Vega [29],  $\epsilon$  Eridani [24], Fomalhaut [30],  $\beta$  Pictoris [77], AU Mic [39]); no discernible asymmetry ( $\tau$  Ceti [25], HD107146 [2], HD181327 [69], HD53143 [36], HD139664 [36]).

face-on disk of TW Hydra [65] from analysis of the emission spectrum which is affected by the fact that the warp prevents light from the star reaching the outer portions of the disk. This method of detecting a warp was possible for TW Hydra which has a classical T Tauri disk, but is not possible for face-on debris disks which are optically thin.

### Spirals

The disk of HD141569 is seen to be significantly extended with dust out to 1200AU where there are two M stars of similar age which are likely to be weakly bound to the star [81]. The radial distribution of dust is peaked at 150 and 250 AU. Optical coronagraphic imaging shows that both of these rings is

a tightly wound spiral [12]. The diffuse emission from 300-1200 AU also forms a more open spiral structure, with one, possibly two arms. Two armed open spiral structure is also reported in younger transition disks, such as AB Aur [46]. Recent observations of Vega suggest that its extended sub-mm emission is condensed into two spirals (Holland et al., in prep.).

### Offsets

The star is not always at the centre of the rings. This effect was first predicted [91], but then later dramatically seen in optical images of the Fomalhaut disk [35]. The Fomalhaut disk is narrow, and its proximity of 7.8 pc allowed the radius to be measured with great accuracy as a function of azimuth. With a mean disk radius of 133 AU, an offset of 15 AU was measured with significant confidence. The centre of the  $\epsilon$  Eridani disk is also seen to be offset [26], however the lower resolution of the sub-mm observations and its more complicated clumpy structure make the interpretation of this measurement less clear. Nevertheless, it is interesting to note that for the cases where such measurements can be made (nearby bright disks), an offset is seen.

### Brightness Asymmetries

The offset effect was first predicted from observations of the HR4796 disk [76]. This edge-on disk was seen to be  $\sim 5\%$  brighter on the NE than the SW side, an asymmetry which was attributed to an offset. However, there are other interpretations of brightness asymmetries, since all of the spiral, offset and clump structures could appear as brightness asymmetries when seen edge-on. In other words, this class is likely another manifestation of one of the other types of structure. Indeed the  $\beta$  Pictoris structure now attributed to a clump (see below) was originally seen as an asymmetry [43]. Likewise, the brightness asymmetry seen in mid- to far-IR images of the Fomalhaut disk [71], and which gets stronger at shorter wavelengths, can likely be attributed to the offset seen in optical images [35]. Other disks with brightness asymmetries include HD32297 [33] and HD15115 [37], for which the asymmetries are particularly pronounced. The latter is an example of a *needle* disk, which is seen to extend to significantly larger distances on one side of the star than the other. It is not clear if this is a brightness asymmetry (and the shorter side extends out to the same distance but at a level below the detection limit) or whether the two sides really are truncated at different outer radii.

### Clumps

The most common type of asymmetry seen in debris disks is a change in brightness with azimuth around the ring, with much of the emission concentrated in one or more clumps. The clearest example of this phenomenon is the

$\epsilon$  Eridani disk which is a narrow ring at 60 AU with a well resolved inner hole [24]. The sub-mm images show four clumps of varying brightness within this ring. The interpretation of this structure has been confounded by the ubiquity of background galaxies which appear randomly across sub-mm images. However, the rapid proper motion of this star, which is at 3.6pc, has allowed non-moving background objects to be identified, with three of the clumps confirmed as real using imaging covering a time-span of  $\sim 5$  years [26]. While the inner hole of the Vega disk is seen less clearly in 850  $\mu\text{m}$  imaging, the emission in this disk, which is being seen close to face-on, is concentrated in two clumps that are equidistant from the star, but asymmetric in brightness [29]. The clumps are confirmed in mm-wavelength interferometry [38, 83], but appear at different locations in 350  $\mu\text{m}$  imaging [51], and not at all in far-IR images [73], although that may be because of the low resolution of these observations. Other disks with clumps include Fomalhaut [30], although this may be a manifestation of the offset,  $\beta$  Pictoris [77], for which a brightness asymmetry appears to be originate in a clump with a sharp inner edge, and AU Mic [48], for which clumps are seen at a range of offsets from the star (although note that given the interpretation of the axisymmetric disk structure [72], all of these clumps are likely to be at the same distance from the star, just seen in projection).

### No detectable asymmetry

Some of the resolved disks from Table 1 exhibit no discernible asymmetry in their structure. These are  $\tau$  Ceti [25], HD107146 [2], HD181327 [69], HD53143 and HD139664 [36], and HD92945 [21]. However, this does not necessarily mean that the disks are symmetrical, since some of these images do not have the resolution and/or sensitivity to detect even large scale asymmetries.

## 3 Debris disk models

The observed radial distribution of dust in debris disks can be explained as a consequence of planetesimal belt dynamics. Here I build up a disk dynamical theory which explains how dust is created in a planetesimal belt, and how the combination of gravity, collisional processes and radiation forces conspire to make the radial distribution of dust vary as a function of grain size.

### 3.1 The planetesimal belt

First it is assumed that the outcome of planet formation was to create a ring of planetesimals at a radius  $r$  and of width  $dr$ . The dominant force acting on these planetesimals is the gravity of the star, and all material within the belt orbits the star. These orbits are defined by their semimajor axis,  $a$ , eccentricity,  $e$ ,



and orbital inclination,  $I$ , along with three angles defining the orientation of the orbit (longitude of pericentre,  $\varpi$ , and longitude of ascending node,  $\Omega$ ), and the position within it (e.g., mean longitude,  $\lambda$ , or true anomaly,  $f$ ). There is a distribution of orbital elements which is assumed to be independent of size for the largest planetesimals. This is not the case during planet formation, wherein larger objects grow rapidly specifically because they have lower eccentricities and inclinations than smaller objects.

The size of planetesimals ranges from some maximum diameter  $D_{\max}$  down to dust of size  $D_{\min}$ , and the size distribution is defined by the amount of cross-sectional area  $\sigma(D)dD$  in each size bin of width  $dD$ ; cross-sectional area is defined such that a spherical particle has an area of  $\sigma = \pi(D/2)^2$ . Taking the size distribution to be described by a power law,

$$\sigma(D) \propto D^{2-3q}, \quad (2)$$

it follows that, as long as the index  $q$  is in the range  $5/3$  to  $2$ , the total amount of cross-sectional area in the belt,  $\sigma_{\text{tot}}$ , is dominated by the smallest objects within it, whereas its mass is dominated by the largest objects.

### 3.2 Collisions

While eccentricities and inclinations of planetesimals are assumed to be small, the resulting relative velocities are large enough that collisions are destructive. This is necessary if dust is to be produced in collisions rather than lost in growth to larger sizes [15].

Within the planetesimal belt collisions between planetesimals of different sizes are continually occurring. The result of such collisions is that the planetesimals are broken up into fragments with a range of sizes. If the outcome of collisions is self-similar (i.e., the size distribution of the fragments is scale invariant), and the range of sizes in the distribution is infinite, then the resulting size distribution has an exponent with  $q = 11/6$  [75]. In this situation the planetesimal belt forms what is known as a collisional cascade, and the size distribution remains constant, with mass flowing from large planetesimals to small grains.

The outcome of a collision depends on the specific incident kinetic energy,  $Q$ . Catastrophic collisions are defined as collisions in which the largest fragment produced in the collision has less than half the mass of original object. In general particles are destroyed in collisions with similar sized particles. In the strength regime,  $D < 150\text{m}$ , the outcome of a collision is determined by the strength of a planetesimal and the specific incident kinetic energy required to destroy it,  $Q_D^*$ , decreases with size. In the gravity regime,  $D > 150\text{m}$ , the fragments created in the collision tend to reassemble under the action of their own gravity, so that a larger input energy is needed to catastrophically destroy a planetesimal, and in that regime  $Q_D^*$  increases with size.

The mean time between collisions for dust in the size range which contributes the majority of the total cross-sectional area in the collisional cascade

can be approximated by [91]:

$$t_{\text{col}} = t_{\text{per}}/4\pi\tau_{\text{eff}}, \quad (3)$$

in years, where  $t_{\text{per}} = a^{1.5}M_{\star}^{-0.5}$  is the orbital period, and  $\tau_{\text{eff}} = \sigma_{\text{tot}}/(2\pi r dr)$  is the effective optical depth of the belt, a (wavelength independent) geometrical quantity that could also be called the surface density of cross-sectional area.

Equation (3) usually applies to the smallest dust grains in the cascade. Larger objects have much longer collisional lifetimes, since there is a lower cross-sectional area in the cascade with sufficient incident energy to induce catastrophic destruction. Their lifetime scales  $\propto D^{5-3q}$  (i.e.,  $\propto D^{-0.5}$  for a canonical collisional cascade size distribution). For details of how the planetesimal strength,  $Q_{\text{D}}^*$ , and orbital eccentricity  $e$  affect the collision lifetime the reader is referred to [90, 94].

### 3.3 Radiation forces

The orbits of small grains are affected by the interaction of the grains with stellar radiation [9]. This is caused by the fact that grains remove energy from the radiation field by absorption and scattering, and then re-radiate that energy moving with the particle's velocity. The resulting radiation force has two components: a radial force, known as radiation pressure, and a tangential force, known as Poynting-Robertson drag (P-R drag). The parameter  $\beta$  is the ratio of the radiation force to that of stellar gravity and is mostly a function of particle size (since both forces fall off  $\propto r^{-2}$ )

$$\beta = F_{\text{rad}}/F_{\text{grav}} = 7.65 \times 10^{-4}(\sigma/m)\langle Q_{\text{pr}} \rangle_{T_{\star}} L_{\star}/M_{\star}, \quad (4)$$

where  $\sigma/m$  is the ratio of a particle's cross-sectional area to its mass (in  $\text{m}^2 \text{kg}^{-1}$ ),  $Q_{\text{pr}}$  depends on the optical properties of the particle, and  $L_{\star}$  and  $M_{\star}$  are in solar units. For large spherical particles  $\beta = (1150/\rho D)L_{\star}/M_{\star}$ , where  $\rho$  is the particle density in  $\text{kg m}^{-3}$ , and  $D$  is in  $\mu\text{m}$ . For smaller particles  $\beta$  tends to a value which is independent of size (see chapter by Li).

#### Radiation pressure

Radiation pressure essentially causes a particle to *see* a smaller mass star by a factor  $(1 - \beta)$ . It is immediately clear that particles with  $\beta > 1$  are not bound and leave the system on hyperbolic trajectories. However, the effect of radiation pressure is also seen at lower values of  $\beta$ , since it means that particles orbiting at the same semimajor axis have different orbital periods, since  $t_{\text{per}} = [a^3/M_{\star}(1 - \beta)]^{0.5}$ .

Most importantly, though, particles created in the destruction of a parent planetesimal have a range of sizes and so  $\beta$ . All particles start with the same

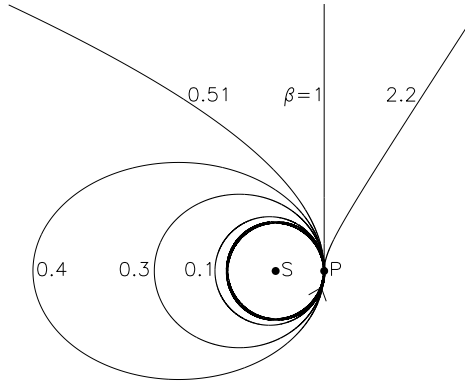


**Fig. 2.** Orbits of particles of different size (and so different  $\beta$ ) created in the destruction of a planetesimal originally on a circular orbit [91]. The collision event occurs at point P. Particles with  $\beta > 0.5$  are on unbound orbits.

position and velocity as the parent, but have different orbital elements because they move in different potentials. For a parent with an orbit defined by  $a$  and  $e$  broken up at a true anomaly  $f$ , the new orbital elements are

$$a_{\text{new}} = a(1 - \beta)[1 - 2\beta[1 + e \cos f][1 - e^2]^{-1}]^{-1}, \quad (5)$$

$$e_{\text{new}} = [e^2 + 2\beta e \cos f + \beta^2]^{0.5} / (1 - \beta) \quad (6)$$

(see Fig. 2). This means that, with a small dependence on where around the orbit the collision occurs, it is particles with  $\beta > 0.5$  that are unbound and leave the system on hyperbolic trajectories. Since particles just above the radiation pressure blow-out limit survive much longer than orbital timescales, this rapid loss causes a truncation in the collisional cascade for small sizes below which  $\beta > 0.5$ .

### P-R drag

P-R drag causes dust grains to spiral into the star while at the same time circularising their orbits (with no effect on the orbital plane). For an initially circular orbit, this means that particles migrate in from  $a_1$  to  $a_2$  on a timescale

$$t_{\text{pr}} = 400M_{\star}^{-1}(a_1^2 - a_2^2)/\beta \quad (7)$$

in years. On their way in particles can be destroyed in collisions with other particles, become trapped in resonance with planets [14], pass through secular resonances, be scattered out of the system by those planets [56], or be accreted onto the planets. If none of these occurs, the particle sublimates close to the star once its temperature reaches above  $\sim 1500$  K. This drag force is thus another potential loss mechanism for dust from the collisional cascade.

It is evident that, since  $t_{\text{pr}} \propto D$  and  $t_{\text{col}} \propto D^{0.5}$ , P-R drag can only be relevant for small particles. Assuming that particles affected by P-R drag contribute little to the total cross-sectional area, the particle size at which P-R drag becomes important can be estimated from equations (3) and (7),

$$\beta > \beta_{\text{pr}} = 5000\tau_{\text{eff}}(r/M_{\star})^{0.5}. \quad (8)$$

Since the smallest grains that may be influenced by P-R drag are those with  $\beta \approx 0.5$  it follows that P-R drag does not affect the evolution of any grains in the disk if  $\tau_{\text{eff}} > 10^{-4}(r/M_{\star})^{0.5}$ , as in this case all bound grains have collisional lifetimes that are shorter than their P-R drag lifetimes.

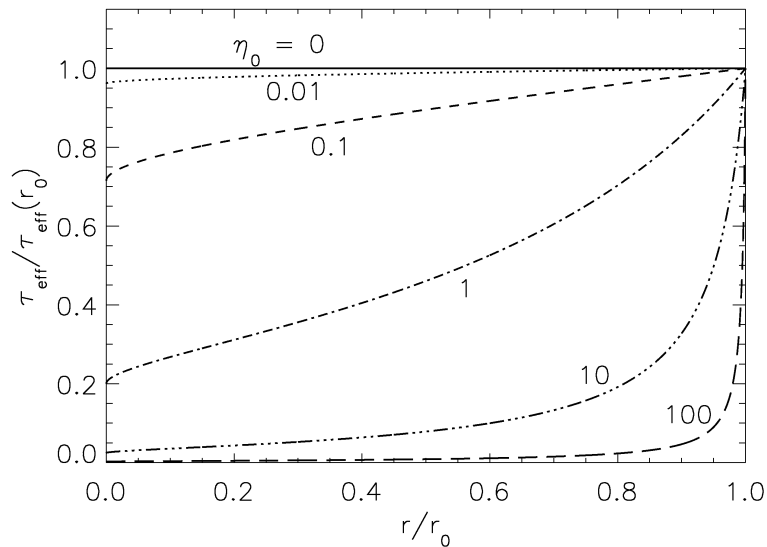


**Fig. 3.** Distribution of surface density for dust grains evolving from a point of origin in a planetesimal belt at  $r_0$  inwards due to P-R drag while also being depleted due to mutual collisions [87].

This back-of-the-envelope calculation was demonstrated more quantitatively in [87] which considered the ideal case of a planetesimal belt which produces grains all of the same size. The spatial distribution of such grains as they evolve due to collisions and P-R drag is given by

$$\tau_{\text{eff}}(r) = \tau_{\text{eff}}(r_0)/[1 + 4\eta_0(1 - \sqrt{r/r_0})], \quad (9)$$

where  $\eta_0 = t_{\text{pr}}/t_{\text{col}} = 5000\tau_{\text{eff}}(r_0)\sqrt{r_0/M_{\star}}\beta^{-1}$  and  $r_0$  is the radius of the planetesimal belt (see Fig. 3). For  $\eta_0 \ll 1$  the majority of the grains make

it to the star without suffering a collision, whereas for  $\eta_0 \gg 1$  the grain population is significantly depleted before the grains make it to the star and so are confined to the vicinity of the planetesimal belt. This model also illustrates how it is not possible to invoke P-R drag to create a large dust population close to the star, since the maximum possible surface density of grains that reach the star in this model is  $5 \times 10^{-5} \beta M_{\star}^{0.5} r^{-0.5}$ .

### 3.4 Disk particle categories

The preceding discussion motivates the division of a debris disk into distinct particle categories which is summarised in Fig. 4:

- **Large grains** ( $\beta \gg \beta_{\text{pr}}$ ): these are unaffected by radiation forces and have the same spatial distribution as the planetesimals;
- **P-R drag affected grains** ( $\beta \approx \beta_{\text{pr}}$ ): these are depleted by collisions before reaching the star;
- **P-R drag affected grains** ( $\beta_{\text{pr}} < \beta < 0.5$ ): these are largely unaffected by collisions and evaporate on reaching the star;
- **$\beta$  critical grains** ( $0.1 < \beta < 0.5$ ): these are on bound orbits and while the inner edge of their distribution follows that of the planetesimals, the outer edge extends out to much larger distances;
- **$\beta$  meteoroid grains** ( $\beta > 0.5$ ): these are blown out on hyperbolic orbits as soon as they are created.

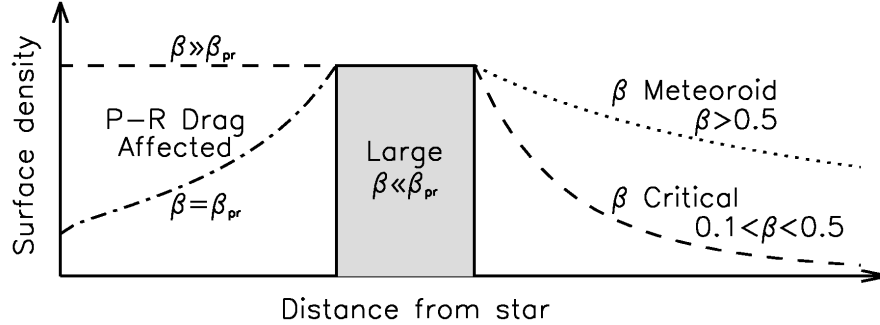


**Fig. 4.** Surface density distribution of particles created in a planetesimal belt [85]. Particles of different sizes have different  $\beta$  and so have different radial distributions. The main categories are: large grains, which have the same distribution as the planetesimals;  $\beta$  critical and  $\beta$  meteoroid grains, which extend much further from the star; and P-R drag affected grains, which extend inwards toward the star.

The presence of different categories in a disk depends on the density of the planetesimal belt. Broadly speaking, the large,  $\beta$  critical and  $\beta$  meteoroid categories are always present (even if the quantities of the latter two relative

to the large grain population are not well known). Thus there are two main types of disk: dense disks that are dominated by collisions which have few P-R drag affected grains, and tenuous disks that are dominated by P-R drag in which P-R drag affected grains are present.

### Collision versus P-R drag dominated disks

The majority of the debris disks that can be detected at present are squarely in the collision dominated regime, since  $\eta_0 \gg 1$  [87]. In the absence of P-R drag the spatial distribution of material becomes very simple. It is even possible to make the simplifying assumption that the  $\beta$  meteoroid population is negligible, because such grains are lost on timescales that are short compared with even the shortest lifetimes in the large grain population. Further ignoring complications due to the eccentricities of the  $\beta$  critical grains, the disk can be modelled as material entirely constrained to the planetesimal belt with a size distribution that extends in a single power law (eq. 2) down to the blow-out limit [90]. While clearly a simplification, this model of the disk is far better than one in which it is comprised of grains all of the same size, since it acknowledges that the dust we see has to originate somewhere. Numerical simulations have also been performed to determine the size and spatial distribution in the collision dominated limit in more detail [79, 78], and further analytical quantification of the distributions in this limit is also possible [72].

The high sensitivity of Spitzer means that more recently relatively low density disks have been detected for which  $\eta_0$  is as low as 1 meaning that P-R drag is expected to sculpt the inner edges of these disks [95]. The effect of P-R drag also needs to be accounted for when studying dust in the solar system, since  $\eta_0 \approx 2 \times 10^{-3}$  in the asteroid belt. It is important to emphasise this point, since it means that the dynamics of dust in the zodiacal cloud is fundamentally different to that of extrasolar systems, albeit in an understandable way. It is also becoming clear that, while stellar wind forces are relatively weak in the solar system providing a drag force  $\sim 1/3$  that of P-R drag (see chapter by Mann), such forces may be important for other stars. While the mass loss rates,  $dM_{\text{wind}}/dt$ , of main sequence stars are poorly known, it is thought that the low luminosity of M stars means that this force may be responsible for the dearth of disks found around late type stars [61]. Since stellar wind forces act in a similar manner to P-R drag, they can be accounted for in the models by reducing  $\eta_0$  by a factor of  $[1 + (dM_{\text{wind}}/dt)c^2/L_\star]$  [32, 53].

Thus, while it is usually the case that the collision dominated approximation is most appropriate, models which describe the distribution of material evolving under the action of collisions and drag forces continue to be of interest. While a study which takes into account the full range of sizes in the disk has yet to be undertaken, it is possible to see that since grains are typically destroyed in collisions with similar sized objects, the outcome of such a model will be similar to assuming that grains of different sizes have spatial distributions that can be characterised by different  $\eta_0$ , with large grains having high

$\eta_0$  and small grains having low  $\eta_0$ . This means that the size distribution would be expected to vary significantly with distance from the star.

### 3.5 Comparison with observations

This model has had considerable success at explaining the observed radial structure of debris disks. For example, using the collision dominated assumption with the dust confined to the planetesimal belt provides an adequate fit to the emission spectrum of disks like that of Fomalhaut [90] for which the radius of its planetesimal belt is well known [30]. It can also explain the structures of the disks which are seen to be considerably extended and to exhibit a gradient in grain size throughout the disk (AU Mic and  $\beta$  Pictoris). These observations are explained as  $\beta$  critical dust being created in planetesimal belts which are closer to the star [4, 3, 72]. Further, the emission spectrum of the TWA7 disk is consistent with the distribution of dust expected from inward migration from the planetesimal belt by stellar wind drag [53].

Thus these studies show that the observed dust distributions can be successfully explained within the framework of a realistic physical model. Such a model is an absolute requirement if any asymmetries seen in the disk structure are to be interpreted correctly, since even the axisymmetric dust distribution is different to that of the planetesimals, which hints that its asymmetric distribution may also differ. On a more basic level, this shows that the location of the dust in a debris disk does not necessarily directly pinpoint the location of the planetesimals.

Despite the successes of the disk dynamical theory it is important to point out that it is not yet a predictive theory. There are too many uncertainties regarding the expected size distribution at very small sizes (e.g., because it depends on the size distribution created in collisions), and regarding the optical properties of those grains and the magnitude of stellar wind drag, to predict how bright a disk known from far-IR measurements (of its large grain population) will appear in scattered light images (which are sensitive to the  $\beta$  critical and  $\beta$  meteoroid grains).

## 4 Interaction between planets and planetesimal belt

Consider now one modification to the planetesimal belt model described in §3, which is that there is a planet orbiting in this system. The gravitational perturbations of that planet will affect the orbits of both the planetesimals and the dust. It turns out that these perturbations are predicted to cause exactly the same set of features as observed in debris disks (Fig. 1).

The planet's perturbations can be broken down, both mathematically and conceptually, into three types: secular, resonant and short period perturbations. For a detailed description of this dynamics the reader is referred to Murray & Dermott (1999) [59]. Its secular perturbations are the long term

consequence of having the planet in the disk, and these perturbations are equivalent to the perturbations from the wire that would be obtained by spreading the mass of the planet around its orbit with a density in accordance with its velocity at each point; they affect all material in the disk to some extent. Its resonant perturbations are the forces which act at specific radial locations in the disk where planetesimals would be orbiting the star with a period that is a ratio of two integers times that of the planet. At such locations the planetesimal receives periodic kicks from the planet which can make such locations either extremely stable or extremely unstable. All other perturbations are short period and can be assumed to average out on long enough timescales, although they are responsible for important processes such as scattering of planetesimals.

#### 4.1 Secular perturbations

To first order a planet's secular perturbations can be separated into two components, one arising from the eccentricity of its orbit, and the other from its inclination. For high eccentricities and inclinations these two components are linked, and here I only consider the low eccentricity and inclination case.

##### Planet eccentricity: spirals and offsets

The consequence of the planet's eccentricity is to impose an eccentricity onto the orbits of all planetesimals in the disk. It does this in such a way that a planetesimal's eccentricity vector, defined by  $z = e \times \exp i\varpi$ , precesses around a circle centred on the forced eccentricity vector,  $z_f$ ; i.e.,

$$z(t) = z_f + z_p(t), \quad (10)$$

where the forced eccentricity is set by a combination of the planet's eccentricity and the ratio of the planetesimal and planet semimajor axes

$$z_f = [b_{3/2}^2(\alpha_{\text{pl}})/b_{3/2}^1(\alpha_{\text{pl}})]z_{\text{pl}}, \quad (11)$$

and the proper eccentricity precesses around a circle the radius of which is determined by the initial conditions

$$z_p(t) = e_p \times \exp i(At + \beta_0), \quad (12)$$

at a fixed rate given by

$$A = 0.25n(M_{\text{pl}}/M_{\star})\alpha_{\text{pl}}\bar{\alpha}_{\text{pl}}b_{3/2}^1(\alpha_{\text{pl}}). \quad (13)$$

In the above equations,  $\alpha_{\text{pl}} = a_{\text{pl}}/a$  and  $\bar{\alpha}_{\text{pl}} = a/a_{\text{pl}}$  for  $a_{\text{pl}} < a$  and  $\alpha_{\text{pl}} = \bar{\alpha}_{\text{pl}} = a/a_{\text{pl}}$  for  $a_{\text{pl}} > a$ , and  $b_{3/2}^s(\alpha_{\text{pl}})$  are the Laplace coefficients. These equations have been given for the case of a system with one planet.



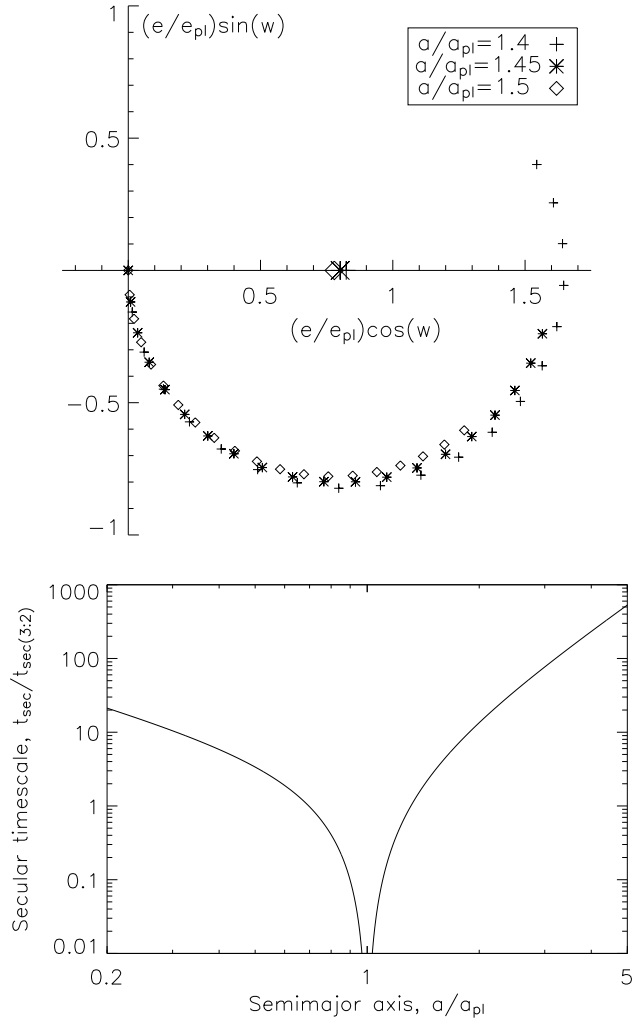


**Fig. 5.** Effect of the secular perturbations of an eccentric planet on planetesimal orbits [88]. **Top** Evolution of the eccentricity vectors of planetesimals at 1.4, 1.45 and  $1.5a_{pi}$ . All vectors start at the origin (circular orbits) and precess around the forced eccentricity imposed on them by the planet. The symbols are plotted at equal timesteps. **Bottom** Precession rate for planetesimals at different distances from the planet. These are given as the timescale to complete one precession ( $2\pi/A$ ) relative to that timescale for planetesimals at  $a = 1.31a_{pi}$  which is given by  $0.651a_{pi}^{1.5} M_{\star}^{0.5}/M_{pi}$ .

However, the same decomposition into forced and proper elements is also true in a system with multiple planets, except that the equations for the forced eccentricity and precession rate  $A$  involve sums over all planet properties [91].

The evolution of a planetesimal's eccentricity vector is illustrated in Fig. 5, which shows how the orbits of planetesimals at 1.4, 1.45 and 1.5 times semi-major axis of the planet evolve if they start on initially circular orbits. This is equivalent to a situation which might arise following the formation of a planet on an eccentric orbit, since the planetesimals would have formed on roughly circular orbits. As well as a small change in forced eccentricity for planetesimals at different distances from the planet, their precession rates are substantially different. This means that the dynamical structure of an extended planetesimal disk evolves following the formation of the planet: planetesimals close to the planet which have completed several precessions can be considered to have eccentricity vectors evenly spread around circles centred on the forced eccentricity, while those further away have pericentre orientations and eccentricities which change with distance from the star.

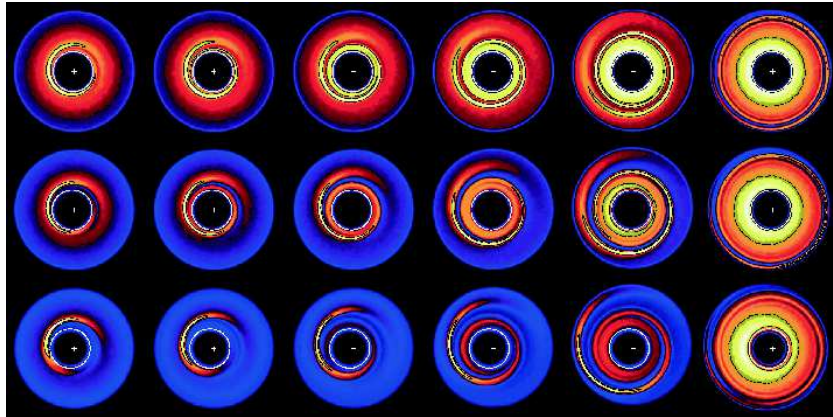


**Fig. 6.** Spatial distribution of planetesimals affected by the secular perturbations of an eccentric planet: spiral structure propagating outward through an extended planetesimal belt outside a planet [88]. The subpanels show, from left to right, snapshots of the disk at times 0.1, 0.3, 1, 3, 10, 100 times the secular precession timescale at  $1.31a_{p1}$  since the perturbing planet was introduced into the disk. From top to bottom the panel show the impact of planets with an eccentricity of 0.05, 0.1 and 0.15.

The resulting dynamical structure can be readily translated into a spatial distribution by creating a model in which planetesimals are distributed randomly in longitude,  $\lambda$ , and with other orbital elements taken from appropriate distributions for the given time. This is shown in Fig. 6 for the planetesimals outside the planet's orbit. It is seen that the planetesimals exhibit spiral structure which propagates away from the planet. A similar spiral structure

is formed in the planetesimal disk interior to the planet, again propagating away from the planet with time.

It is possible that the effect seen in Fig. 6 may be the explanation for the tightly wound spiral structure seen at 325 and 200 AU in the HD141569 disk [12]. Since the rate at which the spiral propagates away from the planet is determined by the planet's mass, this means that the observed structure allows the planet's mass to be estimated, assuming the time since the planet formed can also be estimated. For HD141569 this results in the putative planet having a mass greater than that of Saturn, given the 5 Myr age of the star. A tightly wound spiral structure is also seen in Saturn's rings [11] which is explained by a similar model in which the secular perturbations arise from the oblateness of the planet (rather than from an eccentric perturber), and the ring material is assumed to have formed in a relatively recent event (rather than with the planet).

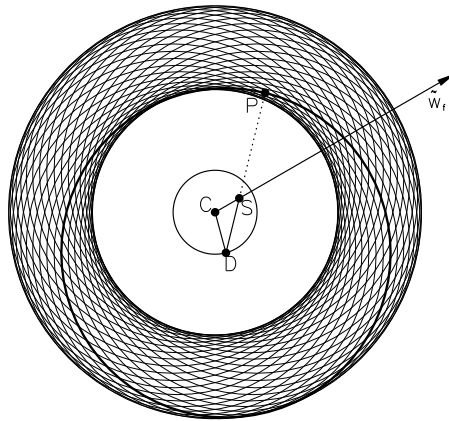


**Fig. 7.** Spatial distribution of planetesimals affected by the secular perturbations of an eccentric planet: offset structure imposed at late times on planetesimals all at the same semimajor axis  $a$  [91]. The planetesimals form a uniform torus around the star at  $S$ , but one which has its centre at a point  $D$  which is offset from the star by a distance  $ae_f$  in the direction of the forced apocentre.

At late times, when the material at the same semimajor axis has eccentricity vectors that are evenly distributed around circles, the resulting disk no longer exhibits spiral structure, but it does exhibit an offset. This is illustrated in Fig. 7, although it is also apparent in Fig. 6 at late times. The offset is proportional to the forced eccentricity imposed on the planetesimals (and so proportional to the planet's eccentricity), with material on the side of the forced pericentre being closer to the star than that on the side of the forced apocentre.

This offset was originally predicted from a brightness asymmetry in the HR4796 disk [91, 76], and was called *pericentre glow* because the asymmetry was thought to arise from the material on the pericentre side being hotter than that on the apocentre side. It was found that the observed brightness asymmetry could have been caused by a planet with an eccentricity as small as 0.02, demonstrating that even moderate planet eccentricities can have observable signatures. However, little information is available from this structure about the mass of the planet, except that it must be sufficiently massive for the pericentres to have been randomised given the age of the star. For HR4796, this means that its putative planet would have to have a mass  $> 10M_{\oplus}$ , although the interpretation of this asymmetry is complicated by the stellar mass binary companion to HR4796A, the orbit of which is unknown at present, but which could also be responsible for an offset of the required magnitude. Nevertheless, an offset has been seen directly in the structure of the Fomalhaut disk [35]. This star also has a common proper motion companion [6], but this is too distant to be responsible for an offset of the observed magnitude.

### Planet inclination: warps

The consequence of secular perturbations caused by the planet’s inclination is directly analogous to the consequence of its eccentricity (§4.1), except that in this case it is the planetesimal’s inclination vector,  $y = I \times \exp i\Omega$ , which precesses around a forced inclination. The precession rate is also the same, except that it is reversed in sign (i.e., the inclination vector precesses clockwise on a figure analogous to Fig. 5). In a system with just one planet the forced inclination vector is simply the orbital plane of the planet ( $y_f = I_{\text{pl}} \times \exp i\Omega_{\text{pl}}$ ). Since the choice of the zero inclination plane is arbitrary it can be set to be the planet’s orbital plane ( $y_f = 0$ ) making it easy to see that at late times, planetesimals at the same semimajor axis will have orbital planes distributed randomly about the orbital plane of the planet. However at early times, should the initial orbital plane of the planetesimals be different to that of the planet at say  $y_{\text{init}}$ , then the situation will be that material close to the planet will be distributed randomly about the planet’s orbital plane  $y_{\text{pl}}$ , while that far from the planet will still be on the original orbital plane  $y_{\text{init}}$ . A smooth transition between the two occurs at a distance from the star which depends on the mass of the planet and the time since the planet formed, much in the same way that spiral structure propagates away from the planet.

This has been proposed as the explanation of the warp in the  $\beta$  Pictoris disk, since other lines of evidence have pointed to a Jupiter mass planet at  $\sim 10$  AU [66, 8], and given the age of the star  $\sim 12$  Myr, it is reasonable to assume that a warp would be seen at  $\sim 80$  AU at the current epoch (if the planet formed very early on). Many observations of the disk, including the warp and the radial distribution (see §2.1), can be explained with such a model [4], although it would be worth revisiting this model in the light of the

observations which showed the warp is less of a smooth transition between two orbital planes and looks more like two distinct disks [20].

This mechanism does not just produce a warp in a young disk. As long as there are two or more planets in the system on different orbital planes a warp would also be seen at late times, once all the planetesimals have precessed so that their distribution is symmetrical about the forced inclination plane, since multiple planets would mean that the forced inclination plane varies with distance from the star (e.g., it is aligned with each of the planet's orbital planes at the semimajor axes of those planets). The zodiacal cloud in the solar system is an example of a warped old disk [91].

## 4.2 Resonant perturbations

Mean motion resonances are locations at which planetesimals orbit the star an integer  $p$  times for every integer  $p+q$  times that the planet orbits the star. The nominal location of a resonance is at a semimajor axis of

$$a_{(p+q):p} = a_{\text{pl}}(1 + q/p)^{2/3}. \quad (14)$$

Planetesimals at a range in semimajor axis about this nominal value may be trapped in resonance, but not all of those in this range are necessarily in the resonance.

### Resonant geometry

The importance of a resonance can be understood purely from geometrical reasons. Fig. 8 shows the path of planetesimals on resonant orbits in the frame co-rotating with the planet. The pattern repeats itself so that the planetesimal always has a conjunction with the planet (i.e., the two are at the same longitude) at the same point in its orbit for  $q = 1$  resonances, or at the same two points in its orbit for  $q = 2$  resonances. This is important because the perturbations to the planetesimal's orbit are dominated by those at conjunction which means that the planetesimal receives periodic kicks to its orbit from the planet which are always in the same direction (if the orbit is unchanged by those perturbations). This is not quite true for the  $p = 1$  resonances, since the cumulative effect of the perturbations around the orbit are also relevant in this case.

The resonant geometry discussed in the preceding paragraph can be used to infer the loopy patterns on a figure such as Fig. 8, but it does not specify the location of the planet with respect to those loops. That is specified by the planetesimal's resonant argument

$$\phi = (p + q)\lambda - p\lambda_{\text{pl}} - q\varpi. \quad (15)$$

The resonant argument is important, since the ratio  $\phi/p$  is the relative longitude of the planet when the planetesimal is at pericentre, an angle which

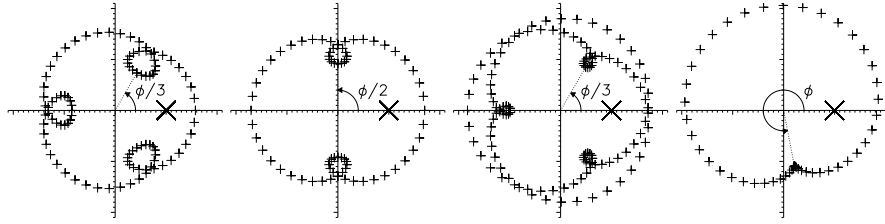


**Fig. 8.** Path of resonant orbits in the frame co-rotating with a planet [86]. On all panels the planet, located at the cross, is on a circular orbit, while the planetesimals' orbits have an eccentricity of 0.3. The planetesimals are plotted with a plus at equal timesteps through their orbit, each point separated by  $1/24$  of the planet's orbital period. The resonances shown are from left to right, with increasing distance from the planet, the 4:3, 3:2, 5:3 and 2:1 resonances.

is noted on Fig. 8; i.e., it determines where along the planetesimal's orbit it receives kicks from the planet's gravity.

The same combination of angles occurs in the planet's disturbing function, and the forces associated with a resonance are those involving the relevant resonant argument [59]. A planetesimal is said to be in resonance if its resonant argument is librating about a mean value (e.g., a sinusoidal oscillation), rather than circulating (e.g., a monotonic increase or decrease). The mean value about which the resonant argument librates is typically  $180^\circ$ , since in this configuration it can be shown that the resonant forces impart no angular momentum to the planetesimal. However, in some instances asymmetric libration occurs, where  $\langle\phi\rangle \neq 180^\circ$ , because the equilibrium solution requires resonant forces to impart angular momentum to the planetesimal (see section on resonant trapping and §5.2). Asymmetric libration also occurs for the  $p = 1$  resonances (e.g., the 2:1 resonance), because in this configuration angular momentum imparted to a planetesimal at conjunction is balanced by the cumulative effect of the resonant forces around the rest of the orbit [58].

### Resonant trapping

While resonances have non-zero width in semimajor axis, their width is finite and they only cover a narrow region of parameter space. Thus if a planet was introduced into an extended planetesimal belt, while planetesimals at suitable semimajor axes might end up trapped in resonance, such planetesimals would be relatively few. However, resonances can be filled by either the planet or the planetesimals' semimajor axes undergoing a slow migration, since when a planetesimal encounters a planet's resonances the resulting forces can cause the planetesimal to become trapped in the resonance. Resonant forces could then either halt the planetesimal's migration, or make it migrate with the planet, thus ensuring that the planetesimal maintains the resonant configuration. For example, it is thought that Pluto and most of the other Kuiper

belt objects that are in resonance with Neptune attained their resonant orbits during an epoch when Neptune’s orbit expanded following its formation [49]. There are a number of mechanisms which can be invoked to cause planets to migrate outward, one of which is angular momentum exchange caused by scattering of planetesimals [27], and another is interaction with a massive gas disk [52].

The question of whether a planetesimal becomes trapped once it encounters a planet’s resonances is determined by two main factors: the mass of the planet and the rate at which the planet or planetesimals are migrating. For example, the probability of a low eccentricity planetesimal being trapped into any given resonance with a planet migrating on a circular orbit is determined by two parameters,  $\mu = M_{\text{pl}}/M_{\star}$  and  $\theta = \dot{a}_{\text{pl}}/\sqrt{M_{\star}/a}$  [86]. It is expected that the eccentricities of the planet and planetesimal orbits would also affect the trapping probability. Another important factor in determining which resonances are filled by planet migration is the initial distribution of the planetesimals with respect to the planet, since this determines how many planetesimals would encounter a given resonance in the course of the migration, given that some may already have been trapped in another resonance. The dominant resonances in the Kuiper belt are the 4:3, 3:2, 5:3 and 2:1 resonances, which can partly be explained by the fact that first order resonances (i.e.,  $q = 1$  resonances) are stronger than second order resonances (i.e.,  $q = 2$  resonances), and so on.

Resonances are important not only for a disk’s dynamical structure, but also for the spatial distribution of material, since Fig. 8 illustrates how planetesimals that are all in the same resonance that have similar resonant arguments would tend to congregate at specific longitudes relative to the planet. That is, while any one planetesimal is on an elliptical orbit, that orbit would take it in and out of regions of high planetesimal density, i.e., clumps. These clumps would appear to be orbiting the star with the planet. The number of clumps formed by resonances is given by  $p$  (e.g., Fig. 8). An important factor in the formation of resonant clumps is the planetesimals’ eccentricities, since the clumps only become pronounced at high eccentricities; resonant planetesimals on circular orbits have an axisymmetric distribution. Once trapped resonant forces can excite the planetesimals so that they become eccentric.

This mechanism was invoked to explain the clumpy structure of Vega’s debris disk (Fig. 9; [86]). In that model two clumps form in the planetesimal distribution because of the migration of a Neptune mass planet from 40 to 65 AU over 56 Myr. As suggested by Fig. 8 the clumps are the result of trapping of planetesimals into the 3:2 resonance, with an asymmetry caused by planetesimals in the 2:1 resonance. The planet’s mass and migration rate are constrained within the model, but not uniquely, since it did not consider the origin of the planet’s migration; e.g., the same structure would arise from a 3 Jupiter mass planet which completed the same migration over 3 Myr. To break this degeneracy models would be required which cause both planet migration and resonant trapping simultaneously, a task which requires significant com-

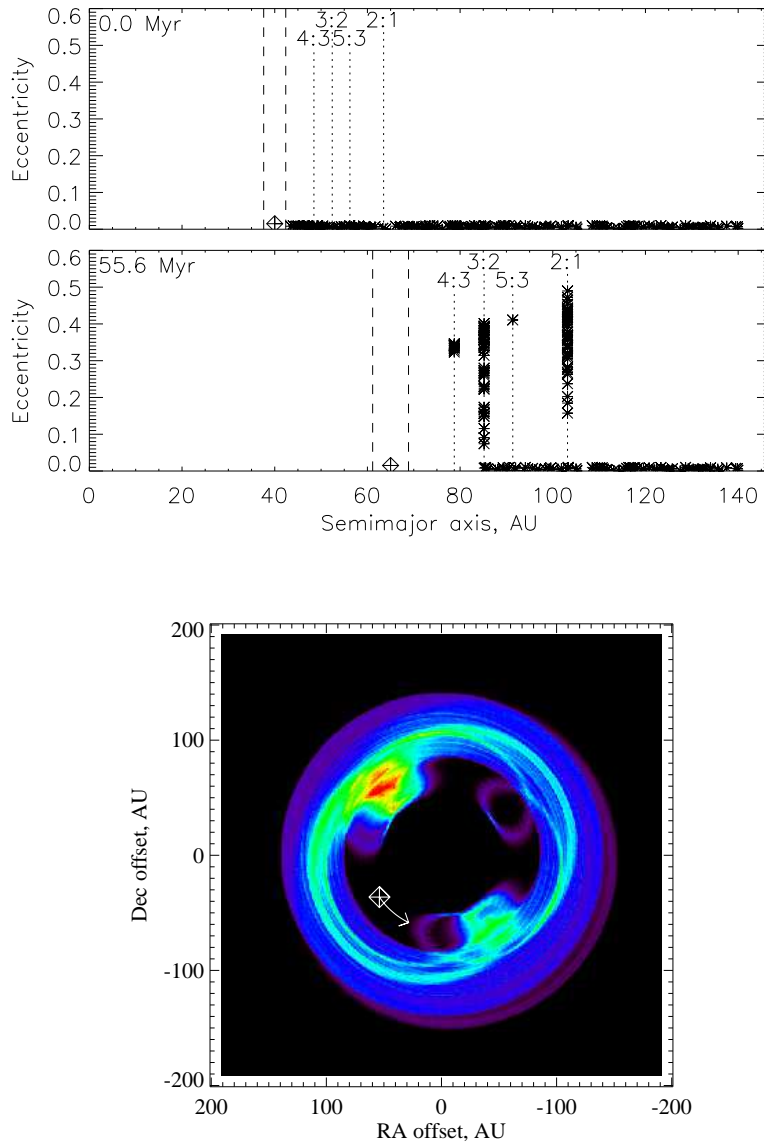


**Fig. 9.** Structure imposed on an initially axisymmetric planetesimal disk by the outward migration of a planet [86]. This model was proposed to explain the clumpy structure of the Vega disk and involves a Neptune mass planet which migrated from 40-65 AU over 56 Myr. **Top** Dynamical structure of the planetesimal disk, eccentricity versus semimajor axis, at the beginning and end of the migration. The planet is shown with a diamond, and the location of its resonances with dotted lines. The chaotic region of resonance overlap is shown with dashed lines. **Bottom** Spatial distribution (surface density) of planetesimals at the end of the migration. The planet is shown with a diamond and the arrow shows its direction of orbital motion.



puting power. Nevertheless, this model shows that observed structures have the potential to tell us not only about the planets in a system, but also about that system's evolutionary history.

The model has made predictions for: **(i)** the location of the planet (none has been found at the level of  $< 3M_{\text{Jupiter}}$ , [54]); **(ii)** the orbital motion of the clumps which should be detectable on decade timescales (these observations will be made in the coming year, and in the meantime marginal detection of orbital motion has been found in the clumpy structure of the  $\epsilon$  Eridani disk, [62]); **(iii)** lower level structure associated with the 4:3 and 5:3 resonances (which may have been seen in  $350 \mu\text{m}$  observations of the disk [51]).

### Resonance overlap

So far I have discussed the stabilising properties of resonances. However, resonances can also be destabilising. As mentioned above, resonances have finite width, and the  $q = 1$  resonances are strongest. There is a region nearby the planet where its first order resonances overlap, and planetesimals in such a region have chaotic orbits and are rapidly ejected [84]. The width of this region is

$$|a - a_{\text{pl}}|/a_{\text{pl}} = 1.3(M_{\text{pl}}/M_{\star})^{2/7}. \quad (16)$$

Instabilities of this type have been invoked to explain the cleared inner regions of debris disks [16], as well as to estimate the location of a planet inside an imaged planetesimal belt [64]. The same planet also imposes eccentricities on the planetesimals at the edge of the resonance overlap region, and the magnitude of those eccentricities is dependent on the mass of the planet, with more massive planets imposing larger eccentricities. Since those eccentricities result in a sloping inner edge, it is also possible to use the sharpness of the inner edge of a dust ring to set constraints on the mass of the planet. In this way the sharp inner edge of the Fomalhaut ring was used to determine that its planet must be less massive than Saturn [64].

## 5 Interaction between planets and dust

The preceding section (§4) dealt specifically with the structures imposed by planets on the planetesimal distribution. This is an important first step, since the dust we see is derived from those planetesimals. However, as discussed in §3, dust dynamics can be significantly different to that of the planetesimals, and so it is not obvious to what extent the dust distribution will follow that of the planetesimals. A model which takes into account the production in collisions of dust with a range of sizes and the subsequent dynamical evolution of that material is usually beyond the scope of current computing (and analytical) capabilities. Such models will likely become more common-place as more detailed observations demonstrate that more sophisticated models are

necessary to explain the observations. For now, the types of structure which dust dynamics would produce can be understood by considering the dynamical evolution of dust grains released from a given planetesimal distribution. Those grains might then be considered to evolve in the absence of collisions, or in an idealised situation where the only collisions which matter are those with grains of similar size (and so which all have the same spatial distribution).

Here I consider the effect of dust grain dynamics on the structures seen in a planetesimal belt in which some of the planetesimals are in resonance with a planet (§5.1), and the structures caused by trapping of dust into planetary resonances (§5.2).

### 5.1 Dust produced from resonant planetesimals

Only the largest dust grains released from a resonant planetesimal remain in that resonance, and the reason is the effect of radiation pressure. First of all, consider the orbits of grains which remain bound to the star ( $\beta < 0.5$ ). Radiation pressure has two effects: it changes the semimajor axis of the dust grain (so that  $a' = a[1 - \beta]/[1 - 2\beta]$  for initially circular orbits), and also the location of the resonance (the resonance for dust is at a lower semimajor axis by a factor  $(1 - \beta)^{1/3}$  than given in equation 14). This means that the larger a particle's  $\beta$  (which typically means the smaller its size, although see §3.3 and chapter by Li) the further it starts from the resonance, and while resonant forces can accommodate this offset by increasing the libration width for large grains, there comes a size at which particles are no longer in resonance. Numerical simulations showed that for the 3:2 resonance the critical size is that for which  $\beta > \beta_{\text{crit}}$ , where

$$\beta_{\text{crit}} = 2 \times 10^{-3} (M_{\text{pl}}/M_{\star})^{0.5}, \quad (17)$$

with a similar threshold for the 2:1 resonance [89]. Since the geometry of Fig. 8 is no longer valid for non-resonant grains, such grains have an axisymmetric distribution.

Next, consider the orbits of dust grains which are released onto hyperbolic orbits (i.e.,  $\beta > 0.5$ ). For  $\beta = 1$  dust no force acts on the grains, and such grains leave the system with a constant velocity (that of the orbital motion of the parent planetesimal) which rapidly approaches radial motion. Assuming that these grains are created at a constant rate, this corresponds to a surface density distribution which falls off  $\propto r^{-1}$ . Since no force acts on the grains, one might naively expect no asymmetry in their distribution. However, their distribution can be non-axisymmetric if they are not produced from an axisymmetric distribution of parent bodies. Collision rates are highest between resonant planetesimals when they are in the clumps, and this means that a greater fraction of the  $\beta > 0.5$  grains created from planetesimal collisions have trajectories which originate in the clumps. The distribution of such grains should thus exhibit spiral structure which emanates from the clumps (since

while the motion of the dust is nearly radial, the source region, the clumps, are in orbital motion around the star). However, not all  $\beta > 0.5$  grains are created in collisions between planetesimals with a clumpy resonant distribution; some originate in collisions between non-resonant grains with  $\beta_{\text{crit}} < \beta < 0.5$ , and so would have an axisymmetric distribution.

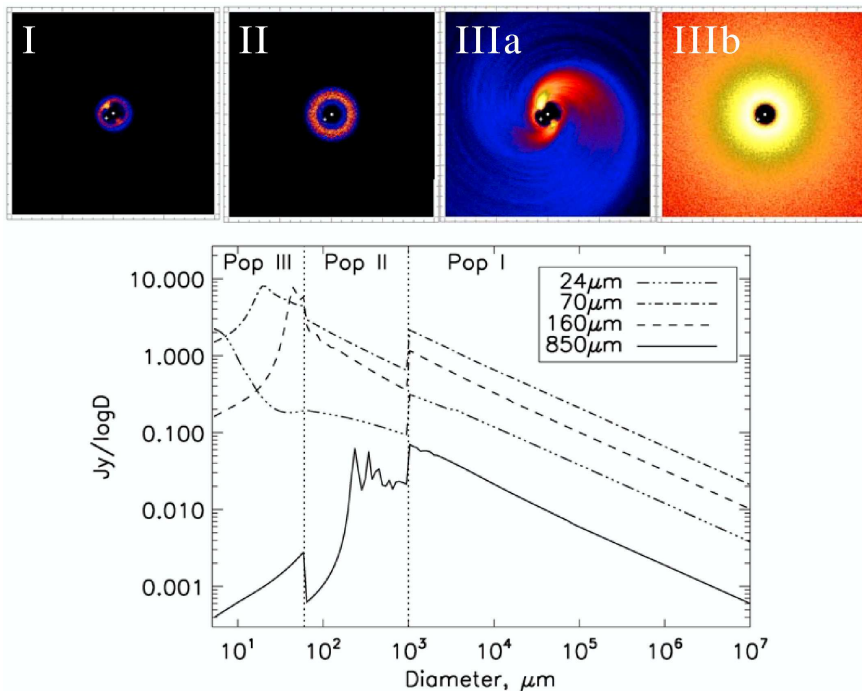


**Fig. 10.** Prediction for the structure of Vega's debris disk [89]. **(Top)** Spatial distribution of dust in different populations: **(I)** large grains, **(II)** intermediate grains, **(IIIa)** small grains (created from large grains), **(IIIb)** small grains (created from intermediate grains). All panels cover the same region ( $\pm 100$  arcsec from the star which is shown by an asterisk at the centre); the location of the planet is shown with a plus. **(Bottom)** Contribution of different grain sizes (and so different populations) to observations in different wavebands. The y axis is flux per log particle diameter, so that the area under the curve is the total flux, and the relative contribution of different grain sizes to that flux is evident from the appropriate region. For the size distribution shown here the mid- to far-IR wavelength observations are dominated by population III grains, while sub-mm observations are dominated by population I grains.

This motivates a division of the dust produced in a resonant planetesimal disk into four populations with distinct spatial distributions: **(I)** large grains  $\beta < \beta_{\text{crit}}$  with a clumpy distribution, **(II)** intermediate grains  $\beta_{\text{crit}} < \beta <$

0.5, with an axisymmetric distribution, **(IIIa)** small grains  $\beta > 0.5$  from population **(I)** particles with extended spiral structure, **(IIIb)** small grains  $\beta > 0.5$  from population **(II)** particles with extended axisymmetric structure. These distributions have been worked out numerically for the model presented in Fig. 9, and the structures expected for the four populations are shown on Fig. 10.

Aside from ascertaining the distribution of different grain sizes, it is important to determine which grain sizes actually contribute to the observation in question. This chapter will not deal specifically with such issues, for which a knowledge of the optical properties of the particles is needed, and for which the reader is referred to the chapter by Li in this book. However, the type of result that is obtained with such an analysis is illustrated in Fig. 10. This shows how observations in different wavebands are sensitive to different grain sizes and to different grain populations, with the shortest wavelengths probing the smallest grains; i.e., the disk would be expected to look different when observed at different wavelengths. For the Vega disk, this is indeed seen to be the case [51], although this does not mean the dynamics of this disk is completely understood, since the prediction for the spiral structure at the shortest wavelengths [89] has yet to be confirmed, and the large observed mass loss rate remains to be explained [73].

The fact that disk structure is expected to be (and is seen to be) a strong function of both grain size and wavelength of observation is good because it means that multiple wavelength observations of the same disk provide a means to test different models for the origin of structure formation. However, it also means that the models are becoming more complicated, and this means that the interpretation of observed structure is no longer straight forward, since there are multiple physical processes that have to be accounted for. For example, it should also be noted that the model described above only took account of the effect of radiation pressure on the dust orbits, and the relative velocity imparted to collisional fragments may also be important [40].

## 5.2 Resonant trapping of dust by P-R drag

Planetary resonances can also sculpt a dust disk even if the parent planetesimals are not trapped in resonance, since the drag forces which act on dust to make it migrate inwards (see §3.3) mean that the dust may have the opportunity to encounter a planet's resonances. Resonant forces can then halt the migration causing a concentration of dust along the planet's orbit known as a *resonant ring*. For the same geometrical reasons as outlined in §4.2, these resonant rings are clumpy.

There are some important subtle differences in the structure of this type of resonant ring compared with the resonant planetesimal rings. One of these is the fact that the libration of  $\phi$  is offset from  $180^\circ$  so that resonant forces can impart angular momentum to the particles to counteract that lost by P-R drag. This means that the loopy patterns on Fig. 8 are not symmetrical

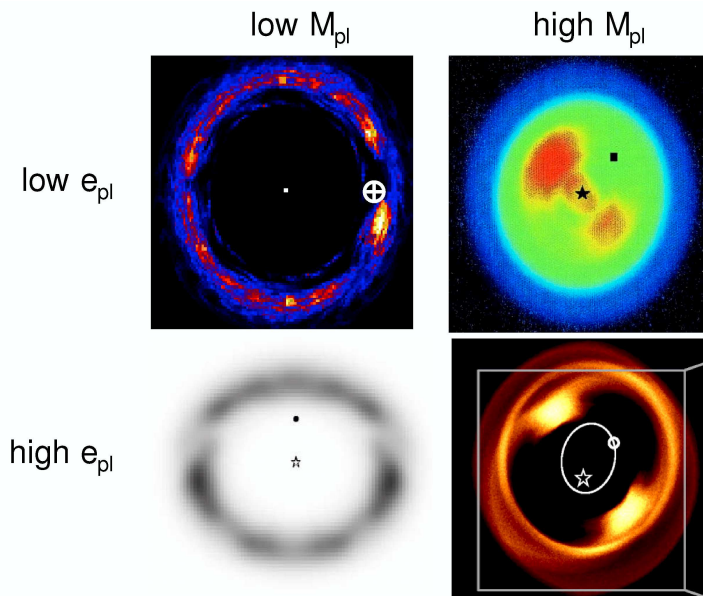


**Fig. 11.** Spatial distribution of dust which has migrated into the resonance of a planet forming a *resonant ring*. The structure of the ring depends on the mass and eccentricity of the planet [41], and examples of the four types of structure are taken from published models: low  $M_{\text{pl}}$ , low  $e_{\text{pl}}$  (model for the Earth’s resonant ring [14]); high  $M_{\text{pl}}$ , low  $e_{\text{pl}}$  (model for the Vega dust ring [60]); low  $M_{\text{pl}}$ , high  $e_{\text{pl}}$  (model for the  $\epsilon$  Eridani dust ring [63]); high  $M_{\text{pl}}$ , high  $e_{\text{pl}}$  (model for the Vega dust ring [83]).

about the planet in such a way that the loop which is immediately behind the planet is closer to the planet than that in front of it. The magnitude of this effect is dependent on particle size ( $\beta$ ). The concentration of all the loops from the different resonances and particle sizes behind the planet causes a clump to follow the planet around its orbit. This is sometimes referred to as a trailing wake. This effect was responsible for the discovery of the first resonant ring, since the zodiacal cloud was found to always be brighter in the direction behind the Earth’s motion than in front of it [14]. This was interpreted as dust trapped in  $q = 1$  resonances close to the Earth (i.e., with  $p > 3$ ) (see top left panel of Fig. 11). The structure of the Earth’s trailing wake will soon be known in great detail, as the infrared satellite Spitzer is currently flying directly through the middle of it. There is no evidence for a resonant ring associated with Mars [42], but recent evidence shows that Venus has a resonant ring [44].

The structure of a resonant ring depends on the mass of the planet, because the resonant forces from a more massive planet are stronger meaning that dust can be trapped into resonances that are further from the planet, e.g., the 3:2 and  $p = 1$  resonance such as the 2:1 and 3:1 resonances (see top

right panel of Fig. 11). The ring structure is also dependent on the planet's eccentricity [41] (bottom panels of Fig. 11). However, one of the most important factors which determines that structure is the spatial distribution of source planetesimals and the size distribution of particles encountering the different resonances, since it is that which determines which resonances are populated. It is not easy to ascertain the expected structure of a resonant ring, since a complete resonant ring model would have to consider the competition between production and destruction in collisions and removal by P-R drag, on top of which some fraction of the particles are trapped in different resonances for varying durations. Needless to say, current models make some approximations, and typically ignore collisions and consider only a relatively narrow range of particle sizes that are assumed to evolve independently [55, 13, 57].

One important point to consider is that for a resonant ring to form in this way the dust must migrate inwards on a timescale that is shorter than the timescale for it to be destroyed in collisions. As discussed in §3.4, the role of P-R drag in affecting the orbits of dust in the disks which are known about at present is negligible, since the collision timescale is short. Thus, while stellar wind drag forces may increase the drag rate for late type stars, the expectation is that resonant rings of this type are not present in the known disks [87, 40]. This serves as a caution that it is dangerous to apply our knowledge of the dynamical structures in the solar system's dust cloud [14, 47] directly to extrasolar systems without first having considered the dust dynamics. However, the example of the solar system also demonstrates that, once we are able to detect more tenuous debris disks, perturbations from Neptune-mass planets will be readily detectable, and it will even be possible to detect structures associated with planets as small as the Earth. In much the same way as it is not yet possible to detect the putative planets around stars like Vega, the dust structures associated with terrestrial planets may also be easier to detect than the planets themselves.

## 6 Conclusions

This chapter has considered the types of structures seen in the dusty debris disks of nearby stars (§2) and how those structures can be used to determine the layout of their planetary systems, in terms of the distributions of both planetesimals and planets. The text has dwelled on the successes of the models at explaining the observed structures, because this illustrates the elements that are essential to any debris disk model if the observations are to be successfully explained (§3), and because we are confident that we understand how a planet would perturb a planetesimal belt in an idealised system comprised of just one planet (§4) and to some extent how to extrapolate that to consider how the planet would affect the observed dust disk (§5). To summarise what we have learned: **(i)** the axisymmetric structure of debris disks can mostly be explained by a model in which dust is created in collisions in a

narrow planetesimal belt and is subsequently acted on by radiation forces; **(ii)** the asymmetric structure of debris disks can mostly be explained by secular and resonant gravitational perturbations from unseen planets acting on the planetesimal belt and dust derived from it.

Knowing the radial location of the planetesimal belts is important because this demonstrates where in a protoplanetary disk grain growth must have continued to km-sized planetesimals [90], and by analogy with the solar system there is reason to believe that the location of the planetesimal belts tells us indirectly the whereabouts of unseen planets, although it is worth bearing in mind that there may be alternative explanations for gaps in the planetesimal distribution related to the physics of the protoplanetary disk. Nevertheless, it appears that where we have the capability to look for detailed disk structure, there is good correspondence between the asymmetric structures observed with those expected if there are planets in these systems. The modelling is also sufficiently advanced that the disk structure can be used to infer information on the properties of the perturbing planets (such as the planet's mass, orbit and even evolutionary history). The planet properties which have been inferred in this way are particularly exciting when compared with those of exoplanets discovered using the radial velocity and transit techniques. Figure 12 shows how the debris disk planets are similar to Uranus and Neptune in the solar system, occupying a unique region of parameter space. This is possible because the large size of debris disks means that the planets perturbing them are most often at large orbital radii, and it is easy for planets as small as Neptune to impose structure on a debris disk. There is also the tantalising possibility that in the future debris disk structures can be used to identify planets analogous to the Earth and Venus in extrasolar systems.

However, while it is incontrovertible that if there are planets present they would impose structure on a disk, the question of whether we have already seen these structures in extrasolar systems is still a matter for debate. In many cases the presence of an unseen planet is the only explanation for the observed structures, but that does not mean that it has to be the right explanation. The problem is that it is hard to confirm that the planets are there, since they lie beyond the reach of radial velocity studies (see Fig. 12). Direct imaging could detect planets at this distance if they were a few times Jupiter mass [54], but not if they are Neptune mass. Thus the onus is on the models to make other testable predictions, and some of these have already been made (such as the orbital motion of the clumpy structures, and the disk structures expected to be seen at different wavelengths) and will be tested in the coming years. If these planets are confirmed, their addition onto plots like that shown in Figure 12 will be invaluable for constraining planet formation models [31].

It is also important to remember that this theory cannot yet predict the quantities of small grains we would expect to see in any given disk. There are too many uncertainties regarding the dust production mechanisms, and it is possible that these processes may differ among stars with, e.g., different dust compositions. Applying dynamical models of the kind presented in §3

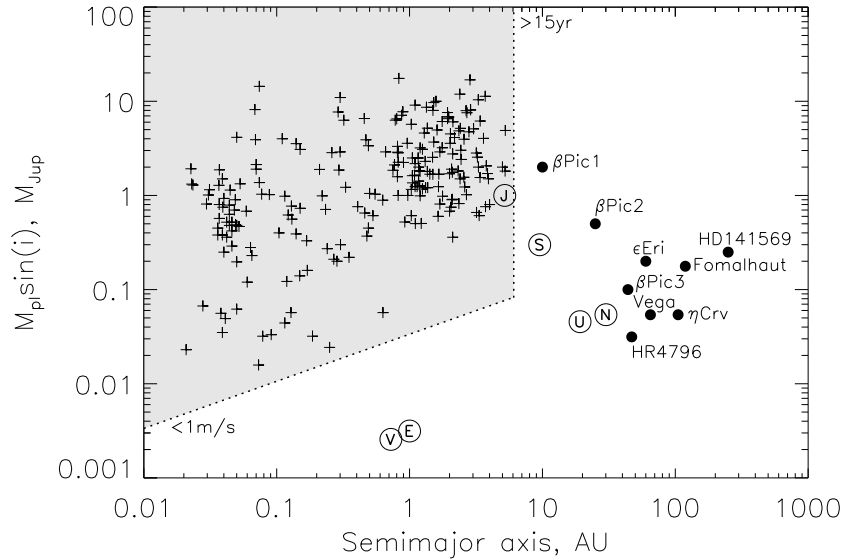


**Fig. 12.** Distribution of planet masses and semimajor axes. Solar system planets are plotted as open circles, and those known from radial velocity and transit studies with a plus (taken from the list on <http://exoplanets.eu> dated 24 May 2007). The shaded region shows the current limits of radial velocity surveys for sun-like stars. Debris disk planets inferred from disk structure (all awaiting confirmation) are shown with filled circles. References for the plotted planet parameters are: HR4796 [91],  $\epsilon$  Eridani [60], Vega [86], HD141569 [88],  $\eta$  Corvi [93], Fomalhaut [64],  $\beta$  Pictoris [19], although it should be noted that these parameters, particularly planet mass, are often poorly constrained.

to a greater number of resolved disk observations will help to understand these differences. However, there is still the possibility that the problem is more fundamental in a way which is best illustrated by the archetypal debris disk Vega. The observed mass loss rate from  $\beta$  meteoroids in this system is  $2M_{\oplus}/\text{Myr}$ , which indicates that this must be a transient, rather than a steady state, component [73]. It is thus possible that the small grain population in debris disks is inherently stochastic, perhaps influenced by input from recent massive collisions [77]. Fortunately it appears that the large grain component of the majority of debris disks is evolving in steady state [95] and so can be understood within the framework described in this chapter, and the same is likely also true for the small grain component (it is just the relative quantities of the different components that is less certain).

However, the possibility must be considered that in some systems the observed dust is transient in such a way that its origin will require a significant



overhaul to the models presented here. For example, there are a few cases of sun-like stars surrounded by hot dust (e.g., §2.1) which cannot be maintained by steady state production in a massive asteroid given the age of the stars [94]. It is not clear what the origin of the transient event producing the dust is. However, it is known that the quantity of planetesimals in the inner solar system has had a stochastic component, notably involving a large influx  $\sim 700$  Myr after the solar system formed in an event known as the late heavy bombardment, the origin of which is thought to have been a dynamical instability in the architecture of the giant planets [22]. So perhaps these systems are telling us about the more complex dynamics of their planetary systems. Given the complexity of planetary systems it seems inevitable that the models presented in this chapter are just the start of a very exciting exploration of the dynamics of extrasolar planetary systems.

## References

1. O. Absil, et al: *Astron. Astrophys.* **452**, 237 (2006)
2. D.R. Ardila, et al: *Astrophys. J.* **617**, L147 (2004)
3. J.-C. Augereau, H. Beust: *Astron. Astrophys.* **455**, 987 (2005)
4. J.-C. Augereau, R.P. Nelson, A.M. Lagrange, J.C.B. Papaloizou, D. Mouillet: *Astron. Astrophys.* **370**, 447 (2001)
5. H.H. Aumann, et al: *Astrophys. J.* **278**, L23 (1984)
6. D. Barrado y Navascues, J.R. Stauffer, L. Hartmann, S.C. Balachandran: *Astrophys. J.* **475**, 313 (1997)
7. D.E. Backman, F. Paresce: Debris disks. In: *Protostars and Planets III*, ed by E.H. Levy, J.I. Lunine (Tucson, Univ. Arizona Press 1993) pp 1253–1302
8. H. Beust, A. Morbidelli: *Icarus* **143**, 170 (2000)
9. J.A. Burns, P.L. Lamy, S. Soter: *Icarus* **40**, 1 (1979)
10. G. Bryden, et al: *Astrophys. J.* **636**, 1098 (2006)
11. S. Charnoz, C. C. Porco, E. Déau, A. Brahic, J.N. Spitale, G. Bacques, K. Baillie: *Science* **310**, 1300 (2005)
12. M. Clampin, et al: *Astron. J.* **126**, 385 (2003)
13. A.T. Deller, S.T. Maddison: *Astrophys. J.* **625**, 398 (2005)
14. S.F. Dermott, S. Jayaraman, Y.L. Xu, B.A.S. Gustafson, J.C. Liou: *Nature*, **369**, 719 (1994)
15. C.P. Dullemond, C. Dominik: *Astron. Astrophys.* **434**, 971 (2005)
16. P. Faber, A.C. Quillen: *Mon. Not. Royal Astron. Soc.* **submitted**, (2006)
17. R.S. Fisher, C.M. Telesco, R.K. Piña, R.F. Knacke, M.C. Wyatt: *Astrophys. J.* **532**, L141 (2000)
18. D.A. Fischer, J.A. Valenti: *Astrophys. J.* **622**, 1102 (2005)
19. F. Freistetter, A.V. Krivov, T.Löhne: *Astron. Astrophys.* **466**, 389 (2007)
20. D.A. Golimowski, et al: *Astron. J.* **131**, 3109 (2006)
21. D.A. Golimowski, et al: In: *Spirit of Lyot 2007*, <http://www.lyot2007.org> (2007)
22. R. Gomes, H.F. Levison, K. Tsiganis, A. Morbidelli: *Nature* **435**, 466 (2005)
23. J.R. Graham, P.G. Kalas, B.C. Matthews: *Astrophys. J.* **654**, 595 (2007)
24. J.S. Greaves, et al.: *Astrophys. J.* **506**, L133 (1998)

25. J.S. Greaves, M.C. Wyatt, W.S. Holland, W.R.F. Dent: *Mon. Not. Roy. Astron. Soc.* **351**, L54 (2004)
26. J.S. Greaves, et al.: *Astrophys. J.* **619**, L187 (2005)
27. J.M. Hahn, R. Malhotra: *Astron. J.* **117**, 3041 (1999)
28. S.R. Heap, D.J. Lindler, T.M. Lanz, R.H. Cornett, I. Hubeny, S.P. Maran, B. Woodgate: *Astrophys. J.* **539**, 435 (2000)
29. W.S. Holland, et al.: *Nature* **392**, 788 (1998)
30. W.S. Holland, et al.: *Astrophys. J.* **582**, 1141 (2003)
31. S. Ida, D.N.C. Lin: *Astrophys. J.* **604**, 388 (2004)
32. M. Jura: *Astrophys. J.* **603**, 729 (2004)
33. P. Kalas: *Astrophys. J.* **635**, L169 (2005)
34. P. Kalas, D. Jewitt: *Astron. J.* **110**, 794 (1995)
35. P. Kalas, J.R. Graham, M. Clampin: *Nature* **435**, 1067 (2005)
36. P. Kalas, J.R. Graham, M.C. Clampin, M.P. Fitzgerald: *Astrophys. J.* **637**, L57 (2006)
37. P. Kalas, M.P. Fitzgerald, J.R. Graham: *Astrophys. J.* **661**, L85 (2007)
38. D.W. Koerner, A.I. Sargent, N.A. Ostroff: *Astrophys. J.* **560**, L181 (2001)
39. J.E. Krist, D.R. Ardila, D.A. Golimowski, M. Clampin, H.C. Ford: *Astron. J.* **129**, 1008 (2005)
40. A.V. Krivov, M. Queck, T.Löhne, M. Sremcevic: *Astron. Astrophys.* **462**, 199 (2007)
41. M.J. Kuchner, M.J. Holman: *Astrophys. J.* **588**, 1100 (2003)
42. M.J. Kuchner, W. T. Reach, M. E. Brown: *Icarus* **145**, 44 (2000)
43. P.O. Lagage, E. Pantin: *Nature* **369**, 629 (1994)
44. C. Leinert, B. Moster: *Astron. Astrophys.* **472**, 335 (2007)
45. A. Li, J.I. Lunine: *Astrophys. J.* **590**, 368 (2003)
46. S.-Y. Lin, N. Ohashi, J. Lim, P.T.P. Ho, M. Fukugawa, M. Tamura: *Astrophys. J.* **645**, 1297 (2006)
47. J.C. Liou, H.A. Zook: *Astron. J.* **118**, 580 (1999)
48. M.C. Liu: *Science* **305**, 1442 (2004)
49. R. Malhotra: *Astron. J.* **110**, 420 (1995)
50. V. Mannings, M.J. Barlow: *Astrophys. J.* **497**, 330 (1998)
51. K.A. Marsh, C.D. Dowell, T. Velusamy, K. Grogan, C.A. Beichman: *Astrophys. J.* **646**, L77 (2006)
52. R.G. Martin, S.H. Lubow, J.E. Pringle, M.C. Wyatt: *Mon. Not. Royal Astron. Soc.* **in press**, (2007)
53. B.C. Matthews, P.G. Kalas, M.C. Wyatt: *Astrophys. J.* **in press**, (2007)
54. S.A. Metchev, L.A. Hillenbrand, R.J. White: *Astrophys. J.* **582**, 1102 (2003)
55. A. Moro-Martín, R. Malhotra: *Astron. J.* **124**, 2305 (2002)
56. A. Moro-Martín, R. Malhotra: *Astrophys. J.* **633**, 1150 (2005)
57. A. Moro-Martín, S. Wolf, R. Malhotra: *Astrophys. J.* **621**, 1079 (2005)
58. R.A. Murray-Clay, E.I. Chiang: *Astrophys. J.* **619**, 623 (2005)
59. C.D. Murray, S.F. Dermott: *Solar System Dynamics* (Cambridge University Press, Cambridge 1999)
60. L.M. Ozernoy, N.N. Gorkavyi, J.C. Mather, T.A. Taidakova: *Astrophys. J.* **537**, L147 (2000)
61. P. Plavchan, M. Jura, S.J. Lipsky: *Astrophys. J.* **631**, 1161 (2005)
62. C.J. Poulton, J.S. Greaves, A.C. Cameron: *Mon. Not. Royal Astron. Soc.* **372**, 53 (2006)

63. A.C. Quillen, S. Thorndike: *Astrophys. J.* **578**, L149 (2002)
64. A.C. Quillen: *Mon. Not. Royal Astron. Soc.* **372**, L14 (2006)
65. A. Roberge, A.J. Weinberger, E.M. Malumuth: *Astrophys. J.* **622**, 1151 (2005)
66. F. Roques, H. Scholl, B. Sicardy, B.A. Smith: *Icarus* **108**, 37 (1994)
67. G. Schneider, et al: *Astrophys. J.* **513**, L127 (1999)
68. G. Schneider, M.D. Silverstone, D.C. Hines: *Astrophys. J.* **629**, L117 (2005)
69. G. Schneider, et al: *Astrophys. J.* **650**, 414 (2006)
70. B.A. Smith, R.J. Terile: *Science* **226**, 1421 (1984)
71. K.R. Stapelfeldt, et al: *Astrophys. J. Suppl.* **154**, 458 (2004)
72. L.E. Strubbe, E.I. Chiang: *Astrophys. J.* **648**, 652 (2006)
73. K.Y.L. Su, et al: *Astrophys. J.* **628**, 487 (2005)
74. K.Y.L. Su, et al: *Astrophys. J.* **653**, 675 (2006)
75. H. Tanaka, S. Inaba, K. Nakazawa: *Icarus* **123**, 450 (1996)
76. C.M. Telesco, et al: *Astrophys. J.* **530**, 329 (2000)
77. C.M. Telesco, et al: *Nature* **433**, 133 (2005)
78. P. Thébault, J.C. Augereau: *Astron. Astrophys.* **in press**, astro-ph/07060344 (2007)
79. P. Thébault, J.C. Augereau, H. Beust: *Astron. Astrophys.* **408**, 775 (2003)
80. C.A. Trujillo, M.E. Brown: *Astrophys. J.* **554**, L95 (2001)
81. A.J. Weinberger, R.M. Rich, E.E. Becklin, B. Zuckerman, K. Matthews: *Astrophys. J.* **544**, 937 (2000)
82. J.P. Williams, J. Najita, M.C. Liu, S. Bottinelli, J.M. Carpenter, L.A. Hillenbrand, M.R. Meyer, D.R. Soderblom: *Astrophys. J.* **604**, 414 (2004)
83. D.J. Wilner, M.J. Holman, M.J. Kuchner, P.T.P. Ho: *Astrophys. J.* **569**, L115 (2002)
84. J. Wisdom: *Astron. J.* **85**, 1122 (1980)
85. M.C. Wyatt: *Signatures of Planets in Circumstellar Disks*. Ph.D. Thesis, University of Florida, Gainesville (1999)
86. M.C. Wyatt: *Astrophys. J.* **598**, 1321 (2003)
87. M.C. Wyatt: *Astron. Astrophys.* **433**, 1007 (2005)
88. M.C. Wyatt: *Astron. Astrophys.* **440**, 937 (2005)
89. M.C. Wyatt: *Astrophys. J.* **639**, 1153 (2006)
90. M.C. Wyatt, W.R.F. Dent: *Mon. Not. Roy. Astron. Soc.* **334**, 589 (2002)
91. M.C. Wyatt, S.F. Dermott, C.M. Telesco, R.S. Fisher, K. Grogan, E.K. Holmes, R.K. Piña: *Astrophys. J.* **527**, 918 (1999)
92. M.C. Wyatt, W.S. Holland, J.S. Greaves, W.R.F. Dent: *Earth Moon and Planets* **92**, 423 (2003)
93. M.C. Wyatt, J.S. Greaves, W.R.F. Dent, I.M. Coulson: *Astrophys. J.* **620**, 492 (2005)
94. M.C. Wyatt, R. Smith, J.S. Greaves, C.A. Beichman, G. Bryden, C.M. Lisse: *Astrophys. J.* **658**, 569 (2007)
95. M.C. Wyatt, R. Smith, K.Y.L. Su, G.H. Rieke, J.S. Greaves, C.A. Beichman, G. Bryden: *Astrophys. J.* **663**, 365 (2007)